

Torque Ripple Reduction Method for SRM based on Mathematical Model considering Voltage Limitation

Takahiro Kumagai, Daisuke Sato, Jun-ichi Itoh
Nagaoka University of Technology
1603-1 Kamitomioka-cho, Nagaoka city Niigata, Japan
Tel., Fax: +81 / (258) – 47.9533.
E-Mail: kumagai_t1125@stn.nagaokaut.ac.jp, itoh@vos.nagaokaut.ac.jp
URL: <http://itohserver01.nagaokaut.ac.jp/itohlab/index.html>

Keywords

«Switched reluctance motor», «Torque ripple reduction», «Instantaneous current control»

Abstract

This paper proposes a torque ripple reduction method for Switched Reluctance Motor (SRM). Large torque ripple occurs in SRM during switching phase interval. In order to reduce the torque ripple, the ideal current waveform, which reduces completely the torque ripple, is applied as a command value controlling the instantaneous torque. In the proposed method, the ideal current waveform is derived by considering voltage limitation based on mathematical model. The algorithm for determining the torque command is introduced to derive current command which is possible to generate by the power supply. In addition, the maximum torque which is possible to output under condition of the zero torque ripple is clarified. A three-phase 18S/12P type SRM is used in simulation and experiment in order to validate the proposed method. As a result, the torque with no torque ripple is achieved by employing the proposed algorithm in the simulation. Furthermore, the fundamental components of the torque ripple is reduced by 91.5% on average by applying the proposed method in the experiment.

I. Introduction

Switched reluctance motor (SRM) has several advantages; rare earth element free, low cost, suitability for high speed, rugged construction, and maintenance free. Therefore, SRM is expected to apply into hybrid electric vehicle (HEV) and electric vehicle (EV). However, a large torque ripple occurs compared with other motors, e.g. an induction motor or a permanent magnetic synchronous motor, due to the use of only the reluctance torque generated by the magnetic saliency. This results in large noise and vibration. In order to solve these problems, many control methods to reduce torque ripple, noise, and vibration have been studied actively with the development of the power electronics technology in recent years [1]-[4].

One-phase excitation mode is used as a general control method [5]. In this method, the motor voltage is applied in order that a current flows into only one set of the winding in accordance with the commutation sequence. However, a large torque ripple occurs because it is impossible to generate sufficiently the torque during the switching phase interval by this method. Therefore, the control method of using two-phase excitation mode, the motor voltage in which is applied in order that a current flows into two sets of the winding during the switching phase interval in order to reduce torque ripple, is proposed [1]-[4]. In the two-phase excitation mode, the ideal current waveform which reduces the torque ripple is derived to apply as a command value controlling the instantaneous torque. In this case, it is necessary to model the magnetic characteristic of SRM which is nonlinear.

Several modeling methods have been proposed so far in order to deal with this nonlinear characteristic. One of the modeling method is to use a look-up table based on the measurement result or the analysis result using finite element method (FEM) [1]-[2]. Nevertheless, this method is time-consuming because it is necessary to build the look-up table of the magnetic characteristic for every single motor in advance. On the other hand, another method is to obtain the magnetic characteristic by deriving a magnetic circuit from the shape of SRM [3]. In this method, the effect of the torque ripple reduction is

limited due to the inaccuracy of the modeling. Besides, neural network algorithm has been applied as this solution [4]. However, it seems that this method is complex and requires a long computation time [6]. In summary, the common disadvantage of those above method is that it is time-consuming in order to optimize the current waveform, because the optimization needs to be repeated many times. In addition, look-up table has to build every times if the motor is changed.

This paper proposes a modeling method by mathematical expression based on only the measured parameters of the magnetic characteristic of SRM in order to avoid the problems of time-consuming and lack of accuracy. The derivation method of the ideal current waveform without repeating tests is proposed by utilizing the mathematical expression.

This paper is organized as follows; first, the derivation method of the ideal current waveform based on the SRM's mathematical model is explained. Next, the algorithm for determining the torque command to derive current command which is possible to generate by the power supply. Finally, the maximum torque which is possible to output under condition of the zero torque ripple is clarified.

II. DERIVING IDEAL CURRENT BASED ON MATHMATICAL MODEL

A. Generated torque in SRM

This subsection describes the relationship between the torque, the current, and the rotor position because the generated torque in SRM is determined by their instantaneous values. Note that SRM generates only reluctance torque. In order to formulate this reluctance torque, the magnetic co-energy is considered. The magnetic co-energy W_c equals to the surface areas surrounded by the magnetization curve and the current axis of the magnetic characteristic, and expressed as in (1),

$$W_c(i, \theta_m) = \int_0^i \Phi(i', \theta_m) di' \quad (1)$$

The reluctance torque per one phase is expressed by the variation of magnetic co-energy W_c according to the change of the rotor position, and expressed as in (2),

$$T(i, \theta_m) = \frac{\partial W_c(i, \theta_m)}{\partial \theta_m} = \frac{\partial}{\partial \theta_m} \int_0^i \Phi(i', \theta_m) di' \quad (2)$$

The derivation of the flux linkage Φ in (2) is important to obtain the instantaneous torque.

Table 1 shows the motor parameters of the investigated SRM. A three-phase 18S/12P type SRM is chosen to the example to investigate.

Fig. 1 shows a magnetic characteristic in the SRM. The magnetic characteristic consists of a linear region limited by a small value of the current and a saturation region with a non-linear characteristic in the range of large current. The flux linkage Φ is a function of the position (electrical angle) θ_e and the current i . Therefore, the flux linkage Φ is expressed by two trigonometric functions in relation to position, where the first function is defined as a linear function expressing the magnetic characteristic of the linear region, and the second function is defined as an exponential function representing the magnetic characteristic of the saturation region.

In the linear region, the relationship between the flux linkage Φ and the current i is expressed as in (3) [7],

$$\Phi(i, \theta_m) = L_u i + f(\theta_e)(L_a i - L_u i) \quad (3)$$

where L_a is the initial aligned stator inductance and L_u is the unaligned stator inductance. Then, the periodic function $f(\theta_e)$ is approximated by the fundamental harmonic and the second-to-tenth-order harmonics of the cosine function as shown in (4),

$$f(\theta_e) = \frac{1 + \cos(\theta_e) + \sum_{n=2}^{10} h_n((-1)^{n-1} + \cos(n\theta_e))}{2(1 + h_3 + h_5 + h_7 + h_9)} \quad (4)$$

where h_n is the content rate of the n-order harmonic component. Next, the rotation electrical angle θ_e is considered in the range of $-\pi$ to 0, where $\theta_e=0$ indicates the alignment state, and $\theta_e=-\pi$ indicates the

complete unalignment state. The relationship between the rotation electrical angle θ_e and the rotation mechanical angle θ_m is expressed as in (5),

$$\theta_e = N_r \theta_m + 2\pi \frac{N_r}{N_s} x \quad (5)$$

where N_r is the number of the rotor's poles, N_s is the number of the stator's poles, and $x=0 \dots (N_s/2-1)$ is the coefficient representing stator's phase. Substituting (3) into (2), the generated torque in the linear region is expressed as in (6),

$$T(i, \theta_m) = \frac{\partial f(\theta_e)}{\partial \theta} \frac{(L_a - L_u) i^2}{2} x \quad (6)$$

In the saturation region, the relationship between the flux linkage Φ and the current i is expressed as in (7),

$$\Phi(i, \theta_m) = L_u i + f(\theta_e) \left[\Phi_{sat} \left\{ 1 - (1 + Ki) e^{-\tau i} \right\} + L_{sat} i - L_u i \right] \quad (7)$$

where L_{sat} is the saturated aligned stator inductance, Φ_{sat} is the aligned saturation flux linkage, and τ is the coefficient which is determined to minimize the sum of the squares of the residuals between the magnetic characteristic and (7) in the alignment state. In order to maintain the continuity of the inductance in the low current range and (3), K is expressed as in (8),

$$K = \tau - \frac{L_a - L_{sat}}{\Phi_{sat}} \quad (8)$$

Substituting (2) into (3) and (7), the generated torque in the saturation region is expressed as in (9),

$$T(i, \theta_m) = \frac{\partial f(\theta_e)}{\partial \theta_m} \left\{ \Phi_{sat} \left(i + \frac{K + \tau + K \tau i}{\tau^2} e^{-\tau i} \right) + \frac{L_{sat} - L_u}{2} i^2 + T_o \right\} \quad (9)$$

Let the current value of the boundary of the linear region and the saturation region be I_0 , the value of the generated torque at the boundary T_0 is expressed as in (10),

$$T_o = \frac{L_a - L_{sat}}{2} I_0^2 - \Phi_{sat} \left(I_0 + \frac{K + \tau + K \tau I_0}{\tau^2} e^{-\tau I_0} \right) \quad (10)$$

Fig. 2 depicts the T - i - θ_m characteristic obtained by calculating the formula $T(i, \theta_m)$ at the values of the current from 60A to 540A and the rotor position. It is observed from Fig. 2 that a required current value for any torque at any rotor position can be calculated. On the other words, the proper current value to reduce the torque ripple can also be calculated from Fig. 2.

TABLE I. MOTOR PARAMETERS OF SRM.

Rated mechanical power P_m	2.3 kW
Rated speed ω_n	2000 r/min
Rated torque T_n	11.0 N
Number of poles	Rotor 12, Stator 18
Winding resistance R	0.011 Ω
Number of coil turns	24 turns

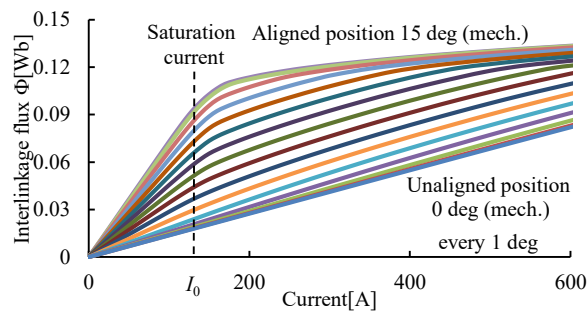


Fig. 1. Magnetization characteristic.

B. Torque sharing function

In this subsection, the control method of each phase's generated torque, which can remove the torque ripple from the motor shaft torque is explained. In this paper, the torque sharing function $f_{Tx}(\theta_m)$ which represents the sharing rate of each phase's generated torque according to the rotor position, is used to derive each phase's ideal current waveform generating the flat instantaneous torque. Generally, the application of the torque sharing function $f_{Tx}(\theta_m)$ is proposed in the conventional derivation method [8].

Fig. 3 shows an example of the torque sharing function. The sum of each phase's generated torque is the constant torque, i.e. a flat torque. Note that the subscript x indicates the phase in the torque sharing function $f_{Tx}(\theta_m)$. In order to generate the command torque for obtaining the flat generated torque, (11) and (12) need to be satisfied,

$$T_{total} = T^* \times \sum_{x=U}^W f_{Tx}(\theta_m) = T \quad (11)$$

$$\sum_{x=U}^W f_{Tx}(\theta_m) = 1 \quad (12)$$

The torque sharing function can have many shapes as long as (12) is satisfied. In Fig.3, θ_{lap} represents the two-phase conduction period and θ_{f0} indicates the initial angle of one-phase conduction period. Since the conduction period of the adjacent phase shifts the angle of π/N_s rad in the mechanical angle in the SRM with the N_s/N_r pole structure, the turn-on angle θ_0 , the ending angle θ_{fc} of the one-phase conduction period, and the turn-off angle θ_c are expressed by (13) as dependent variables of θ_{lap} and θ_{f0} ,

$$\theta_0 = \theta_{f0} - \theta_{lap}, \theta_{fc} = \theta_0 + \frac{\pi}{N_s}, \theta_c = \theta_{f0} + \frac{\pi}{N_s} \quad (13)$$

Therefore, the torque sharing function $f_{Tx}(\theta_m)$ can be determined as the independent variable of θ_{lap} and θ_{f0} . The torque sharing function becomes unity during the one-phase conduction period from θ_{f0} to θ_{fc} , which implies that the torque is generated by only one phase. On the other hand, various functions can be selected during the two-phase conduction period from θ_0 to θ_{f0} . In this paper, the cosine function is utilized in order to avoid a steep rise [8]. Therefore, the torque sharing function used in this paper is expressed as in (14),

$$f_{Tx}(\theta_m) = \begin{cases} \frac{1}{2} \left\{ \cos\left(\frac{\theta_m - \theta_{f0}}{\theta_{lap}}\right)\pi + 1 \right\} & \theta_0 \leq \theta_m \leq \theta_{f0} \\ 1 & \theta_{f0} \leq \theta_m \leq \theta_{fc} \\ \frac{1}{2} \left\{ \cos\left(\frac{\theta_m - \theta_{fc}}{\theta_{lap}}\right)\pi + 1 \right\} & \theta_{fc} \leq \theta_m \leq \theta_c \\ 0 & \text{otherwise} \end{cases} \quad (14)$$

If the generated torque of each phase is controlled exactly by multiplying (14) to the torque command T^* , the torque ripple can be completely removed from the motor shaft torque.

C. Derivation of ideal current waveform

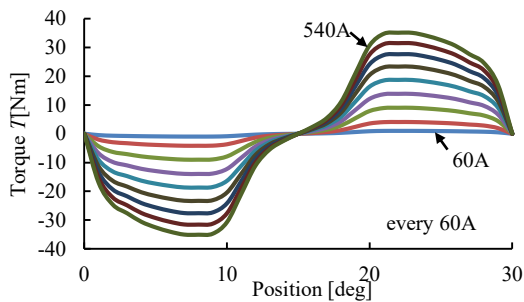


Fig. 2. T - i - θ_m characteristic.

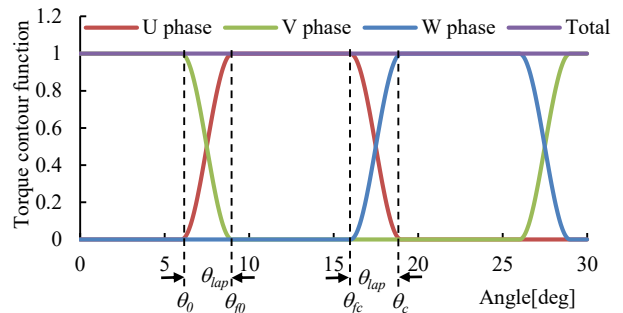


Fig. 3. Torque sharing function.

In this subsection, the derivation method of the ideal current waveform from the T - i - θ characteristic and the torque sharing function is explained. The applied sharing command torque $T^*(\theta_m)$ is calculated from command torque T^* and f_{Tx} and express as $f_{Tx}T^*$. The derivation method of command current to realize $T^*(\theta_m)$ for any rotor position is explained as following.

In order to obtain the flat torque, the generated torque should be controlled exactly to the sharing command torque. Consequently, the following (15) should be satisfied.

$$T(i^*, \theta_m) = T^* f_{Tx}(\theta_m) \quad (15)$$

Then, the instantaneous command current value is calculated from (15). If the current completely follows the command current, the generated torque becomes theoretically a constant value. Next, in the linear region, substituting (6) into (15), the command value $i^*(\theta_m)$ of the ideal current waveform is expressed as in (16),

$$i^*(\theta_m) = \sqrt{\frac{2T^*}{L_a - L_u}} \sqrt{\frac{f_{Tx}(\theta_m)}{\frac{\partial f(\theta_e)}{\partial \theta_m}}} \quad (16)$$

On the other hand, in the saturation region, the command value $i^*(\theta_m)$ of the ideal current waveform can be calculated from (15) based on (9) by Newton's method.

III. VOLTAGE LIMITATION FOR IDEAL CURRENT CONTROL

A. Maximum controllable current gradient

The current command which is possible to generate by the power supply is limited. Therefore, the derivation method of the ideal current waveform responding to the voltage limitation is explained.

Fig. 4 shows the circuit diagram of the multiple phase half bridge inverter which is generally used as the driving circuit for SRM. In general, the hysteresis comparator is used for the current control. In this control method, the switch S_1 is turned off in order that the current circulates through D_1 when the current exceeds an upper threshold. Then, S_1 and S_2 are turned on in order that the current is supplied from the power supply when the current falls below a lower threshold. The motor current is regulated to the command value by repeating the ON/OFF operation. However, it should be noted that the current gradient is limited by the inductance of SRM and DC voltage of the inverter. On the other words, it is impossible for the current to follow the current command, the gradient of which surpasses the limit. Therefore, when deriving the ideal current waveform, it is necessary that the ideal current waveform's gradient should not surpass the maximum current gradient.

First, the maximum gradient which can be followed by the current is derived from the differential equation of SRM at the element's state of ON or OFF. The differential equation of SRM is expressed as in (17),

$$\frac{d\Phi(i, \theta_m)}{dt} + Ri = E_d \quad (17)$$

where Φ is the flux linkage, E_d is the power supply voltage, and R is the winding resistance. The left-side first term of (17) is rewritten into the partial differential equation as in (18) because the flux linkage Φ is the function of the current i and the rotor position θ_m ,

$$\frac{d\Phi(i, \theta_m)}{dt} = \frac{\partial \Phi}{\partial i} \frac{\partial i}{\partial t} + \frac{\partial \Phi}{\partial \theta_m} \frac{\partial \theta_m}{\partial t} = \frac{\partial \Phi}{\partial i} \frac{\partial i}{\partial t} + \frac{\partial \Phi}{\partial \theta_m} \omega \quad (18)$$

The maximum gradient is then derived from (17) and (18). When the current is supplied from the power supply at the element's state of ON, the change rate of the current, i.e. the maximum command current gradient, is expressed as in (19),

$$\frac{\partial i}{\partial t} = \frac{E_d - \frac{\partial \Phi}{\partial \theta_m} \omega - Ri}{\frac{\partial \Phi}{\partial i}} \quad (19)$$

When the current flows to the power supply at the element's state of OFF, the change rate of the current is then expressed as in (20),

$$\frac{\partial i}{\partial t} = \frac{-E_d - \frac{\partial \Phi}{\partial \theta_m} \omega - Ri}{\frac{\partial \Phi}{\partial i}} \quad (20)$$

B. Margin of current gradient

In this subsection, in order to regulate the current to the command current, the appropriation method of the variables θ_{f0} and θ_{lap} , which determine the two-phase period, is explained.

The margin M is defined as the difference between the maximum current change rate and the ideal current change rate. When the margin M is positive, the current to achieve the flat torque can be generated. Otherwise, the flat torque cannot be achieved. If the influence of the speed electromotive force is ignored for simplicity, the angle for minimizing M is either the initial angle of the one-phase conduction period or the turn-off angle. The margin M is calculated from the characteristic of the linear region in both cases because the current is around zero at those angles. Deriving the equation (16) with respect to time, the gradient of the ideal current waveform in the linear region is expressed as in (21),

$$\frac{\partial i}{\partial t} = \frac{1}{\omega} \sqrt{\frac{T^*}{2(L_a - L_u)}} \times \left\{ \frac{1}{\sqrt{f_{Tx}}} \frac{\partial f_{Tx}}{\partial \theta_m} \left(\frac{\partial f(\theta_e)}{\partial \theta_m} \right)^{-\frac{1}{2}} - \sqrt{f_{Tx}} \left(\frac{\partial f(\theta_e)}{\partial \theta_m} \right)^{\frac{3}{2}} \frac{\partial^2 f(\theta_e)}{\partial \theta_m^2} \right\} \quad (21)$$

When the current rises, substituting (3) into (19) and (21), the margin M_f is expressed as in (22),

$$M_f = \frac{E_d}{L_u + f(\theta_{f0} - \theta_{lap})(L_a - L_u)} - \frac{\omega \pi}{\theta_{lap}} \sqrt{\frac{T^*}{2(L_a - L_u)}} \left(\frac{df(\theta_{f0} - \theta_{lap})}{d\theta_m} \right)^{-1/2} \quad (22)$$

On the other hand, when the current falls, substituting (3) into (20) and (21), the margin M_l is given by (23),

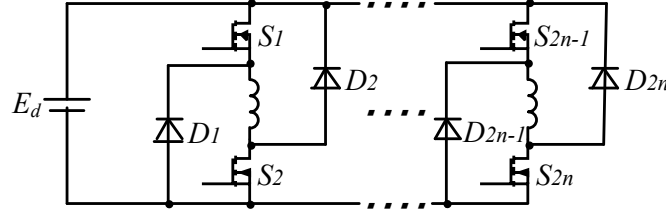


Fig. 4. Multiple phase inverter.

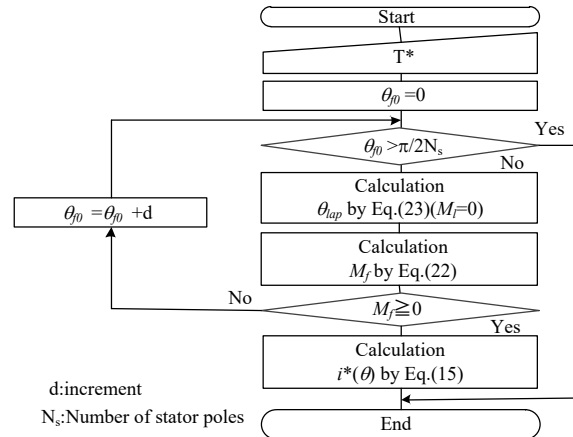


Fig. 5. Generation flow for ideal current waveform.

$$M_l = \frac{E_d}{L_u + f(\pi/N_r + \theta_{f0})(L_a - L_u)} - \frac{\omega\pi}{\theta_{lap}} \sqrt{\frac{T^*}{2(L_a - L_u)}} \left(\frac{df(\pi/N_r + \theta_{f0})}{d\theta_m} \right)^{-1/2} \quad (23)$$

Fig. 5 shows the algorithm to maximize the torque under the condition of the zero torque ripple. In order to derive the ideal current waveform, θ_{lap} is determined with $M_f \leq 0$ by adjusting θ_{f0} when $M_l = 0$.

IV. Simulation and experimental Results

A. Validation of proposed algorithm

The validation of the proposed method is confirmed by simulation. A three-phase 18S/12P type SRM is used. The hysteresis comparator is employed as the current control. The maximum hysteresis error is designed to be small enough to evaluate the torque ripple caused only by the follow or non-follow of the current to the ideal current waveform.

Fig. 6 shows the comparison between the ideal command current's gradient and the maximum gradient. The steps to derive the ideal command current's gradient is that, first let $M_l = 0$, then varying θ_{f0} to calculate θ_{lap} which satisfies $M_f \leq 0$. As shown in Fig. 6, the ideal command current's gradient which can be followed in the latter half of the conduction period, i.e. the period when the current falls, can be calculated by (23).

Fig. 7 shows the relationship between θ_{f0} and M_f when varying the value of θ_{f0} during the former half of the conduction period, i.e. the period when the current rises. Note that at each value of θ_{f0} , first θ_{lap} is derived by (23) when $M_l = 0$, then the margin M_f is calculated by substituting the values of θ_{f0} and θ_{lap} into (22). As shown in Fig. 7, the region where $M_f \geq 0$ represents the values of θ_{f0} where the current can be regulated to the ideal current in order to generate the flat torque. On the other hand, the region where $M_f < 0$ represents the values of θ_{f0} where the current cannot be regulated to the ideal current.

Fig. 8 shows the ideal command currents, the currents, and generated torque in two cases as shown in Fig. 7, where the current can or cannot be regulated to the ideal current. As shown in Fig. 8(a), a large torque ripple occurs when the current cannot follow the command current, because the ideal command current's gradient is higher than the maximum gradient, i.e. the negative margin M_f . On the other hand, as shown in Fig. 8(b), the torque without torque ripple is achieved when the current can follow the command current because the ideal command current's gradient is lower than the maximum gradient, i.e. the positive margin M_f . The validation of the proposed method is confirmed by these results.

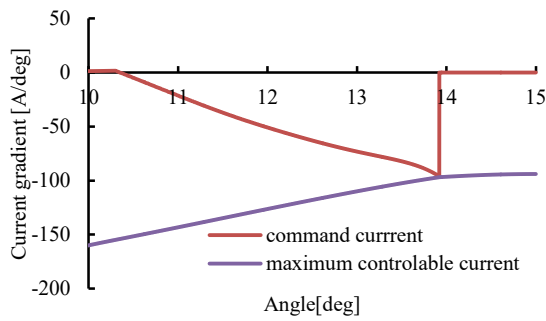


Fig. 6. Current gradient in latter half of conduction period.

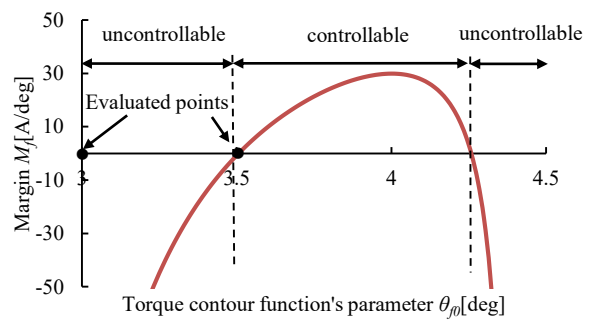
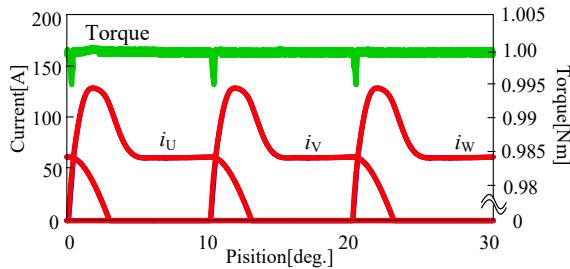
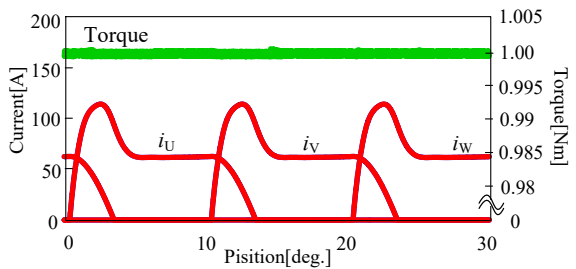


Fig. 7. Margin in former half of conduction period.



(a) Uncontrollable condition ($\theta_{f0} = 3.00$ [deg]).



(b) Controllable condition ($\theta_{f0} = 3.51$ [deg]).

Fig. 8. Current waveform and Output torque.

B. Effectiveness evaluation

The effectiveness of the proposed method is confirmed by experiment. In order to realize high-speed current control and reduce the torque ripple caused by the hysteresis error, current-hysteresis controller is constructed by analog circuit and the current command value i^* of the ideal current waveform is calculated by digital signal processor (DSP) and field-programmable gate array (FPGA).

Fig. 9 shows the currents when applying one-phase excitation mode used as a general mode and proposed method. In this evaluation, command torque T^* is 1.0Nm and rotation speed N is 600rpm.

Fig. 10 shows the harmonic components of the generated torque under the same conditions as Fig. 9. Large torque ripple occurs in SRM during switching phase interval. Therefore, the fundamental frequency of the torque ripple is $3N_rN/60=360\text{Hz}$ in the experimental condition. As shown in the Fig. 10, the fundamental components of torque ripple is reduced from 0.127Nm to 0.011Nm by applying the proposed method. In addition, the second components is reduced from 0.137Nm to 0.042Nm.

Fig. 11 shows the fundamental components and the second components of the generated torque at from $T^*=0.2\text{Nm}$ to $T^*=1.2\text{Nm}$. As shown in Fig. 11, the fundamental components of the torque ripple is reduced by 91.5% on average by applying the proposed method. On the other hand, the effectiveness on the second components of the torque ripple is lower than that on the fundamental components. This is because the torque ripple caused by model inaccuracies occurs especially in both cases that the current falls and rises, i.e. the frequency of the torque ripple caused by model inaccuracies is twice as high as that of the torque ripple caused during switching phase interval.

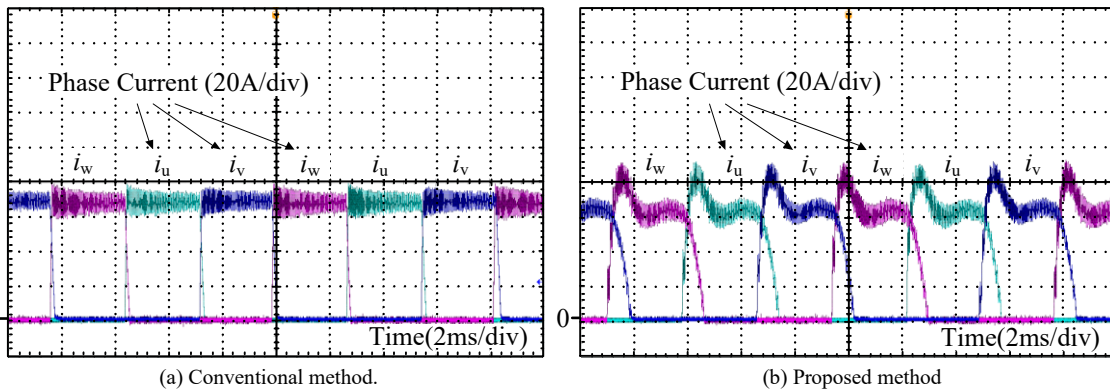


Fig. 9. Current waveform at $T^*=1.0\text{Nm}$, $N=600\text{rpm}$

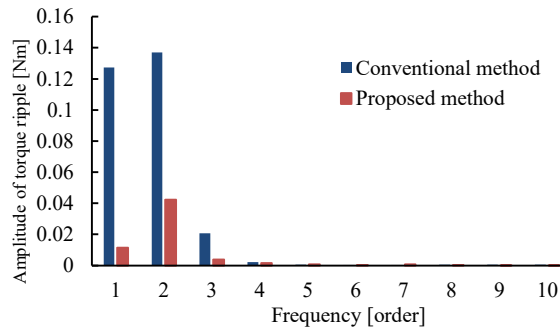


Fig. 10. Harmonic components of the generated torque at $T^*=1.0\text{Nm}$, $N=600\text{rpm}$.

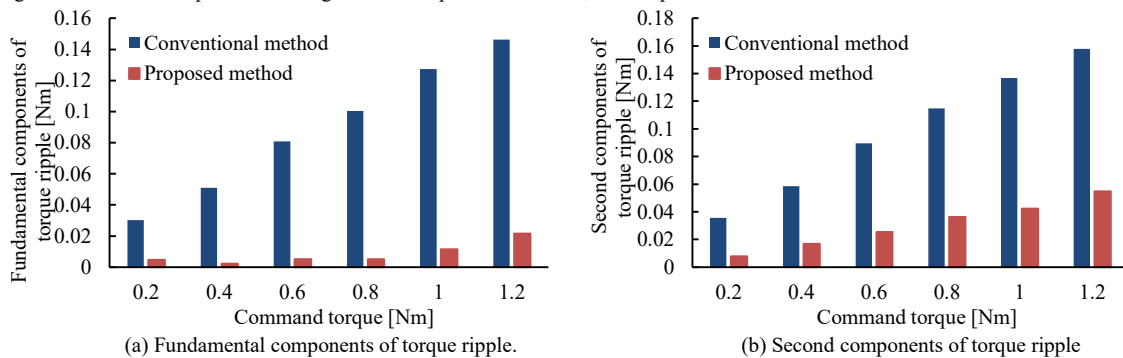


Fig. 11. Characteristics of command torque and harmonic components of the generated torque. By the employment of the proposed method, the fundamental components of torque ripple is reduced by 91.5% and the Second components of torque ripple is reduced by 29.5% on average.

C. Clarification of maximum torque command

The algorithm shown in Fig.6 is the method for deriving the torque sharing function's parameter considering the power supply voltage, when the flat torque can be achieved. In contrast, it is possible to derive the limit of the command torque, which can be completely followed to obtain the flat torque under any condition of the power supply voltage, by comparing the value of M_l when varying the value of T^* .

Fig. 12 shows the relationship between θ_{f0} and M_f when varying the value of T^* . As shown in Fig. 12, $\max(M_f)=0$ is reached with $T^*=1.08$ Nm. Therefore, the current cannot follow the command current if T^* is more than 1.08 Nm, which implies that the flat torque cannot be achieved at the torque above 1.08 Nm. On the other hand, the conditions when the flat torque can be obtained, can be derived by the proposed algorithm if T^* is less than 1.08 Nm.

D. Maximum command torque with different poles

In order to discuss the optimal shape design for the proposed method, the maximum torque achieving zero ripple is compared with several motors having different number of poles. In particular, 6S/4P type, 12S/8P type, and 18S/12P type SRMs are evaluated.

Fig. 13 shows SRMs with different number of poles. Note that the motors are designed to have the same parameters such as; structure, output power, driven supply voltage, and space factor. Furthermore, the ratio of pole pitch and pole arc is set to be similar at the pole shape design step. The smaller the initial aligned stator inductance is, the more the number of poles becomes. It is observed that when the magnetic path length is shorter, and the cross-sectional area is bigger, the magnetic resistance becomes larger.

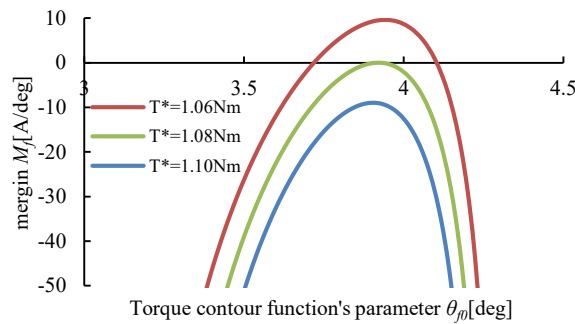


Fig. 12. Evaluation of maximum controllable torque.

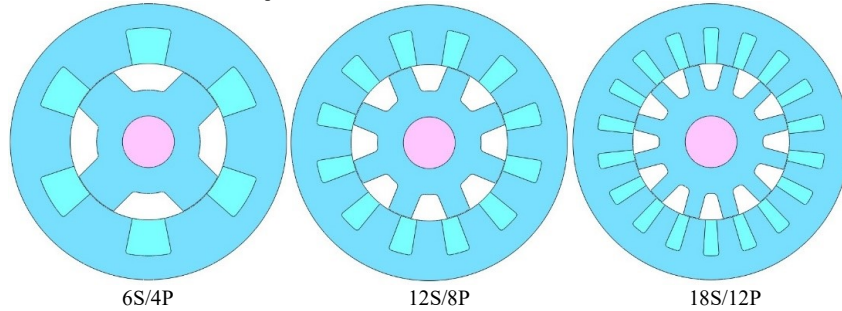


Fig. 13. Motors having different number of poles.

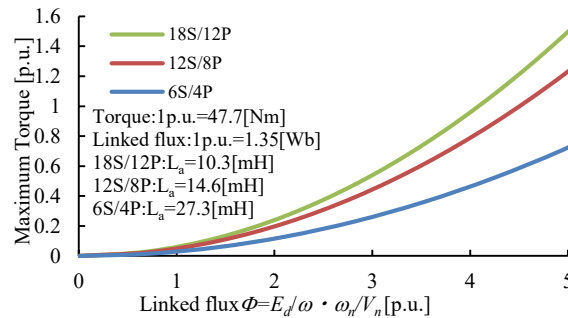


Fig. 14. Comparison of maximum controllable torque with motors having different number of poles.

Fig. 14 shows the relationship between the flux linkage generated by the power supply voltage and the maximum torque T_{max} with the zero torque ripple in the motors having different number of poles. T_{max} is directly proportional to the square of flux linkage. Therefore, T_{max} is directly proportional to the square of the power supply voltage and inversely proportional to the square of the rotation speed. Besides, the more the number of poles are, the larger T_{max} becomes. This is because the initial aligned stator inductance is smaller. Therefore, the motor design with many multipolar is advantageous if the torque with the small ripple is required.

V. Conclusion

This paper proposed the derivation method of the ideal current waveform based on SRM's mathematical model. In the proposed method, a design algorithm was employed to determine the proper torque command to derive current command which is possible to generate. Finally, the maximum torque which was possible to generate under condition of the zero torque ripple was clarified. As a result, the maximum torque was directly proportional to the square of the power supply voltage and inversely proportional to the square of the rotation speed.

References

- [1] Hiroki Ishikawa, Yoshinobu Kamada, Haruo Naitoh: "Instantaneous Current Profile Control for Flat Torque of Switched Reluctance Motors" *Denki Gakkai Ronbunshi*, vol.125-D, no.12, pp.1113-1121 (2005).
- [2] Khwaja M. Rahman, Steven E. Schulz: "High-Performance Fully Digital Switched Reluctance Motor Controller for Vehicle Propulsion", *IEEE Trans. on Industry Applications*, vol.38, no.4, pp1062-1071(2002).
- [3] Jean-Yves Le Chenadec, Marc Geoffroy, Bernard Multon, Jean-Claude Mouchoux: "Torque ripple minimization in Switched Reluctance Motors by optimisation of current wave-forms and of tooth shape with copper losses and "V.A.Silicon" constraints", *ICEM'94*, vol.2, pp.559-564 (1994).
- [4] Z. Lin, D. S. Reay, B. W. Williams, and X. He: "Torque ripple reduction in switched reluctance motor drives using B-spline neural networks", *IEEE Trans. on Industry Applications*, vol. 42, no.6, pp.1445-1453 (2006).
- [5] Michael T. DiRenzo: "Switched Reluctance Motor Control – Basic Operation and Example Using the TMS320F240" Texas Instruments Incorporated, Application Report, SPRA420A (2000).
- [6] M. Brown, K. M. Bossley, D. J. Mills, and C. J. Hams, "High dimensional neurofuzzy systems: Overcoming the curse of dimensionality," in *Proc. IEEE International Conf. on Fuzzy Systems*, vol.4, pp.2139-2146 (1995).
- [7] T. Kenjo: "Switched Reluctance Motor", Nikkan Kogyo Shimbun company (2012).
- [8] Hiroaki Makino, Takashi Kosaka, Shinya Morimoto, Motomichi Ohto, Nobuyuki Matsui: "Instantaneous Current Profile Control of Four-Phase SR Motor for Industrial Servo Drives", *IEEE Trans. on Industry Application*, Vol.135, no.6, pp.711-717 (2015).